

Thermodynamic Spin Glass Phase Induced by Weak Random Exchange Disorder in a Classical Spin Liquid: the Case of the Pyrochlore Heisenberg Antiferromagnet

Ka-Ming Tam,¹ Adam J. Hitchcock,¹ and Michel J. P. Gingras^{1,2}

¹*Department of Physics and Astronomy, University of Waterloo, Waterloo, ON, N2L 3G1, Canada*

²*Canadian Institute for Advanced Research, 180 Dundas Street West, Suite 1400, Toronto, ON, M5G 1Z8, Canada*

(Dated: November 17, 2018)

The glassy behavior observed in the pyrochlore magnet $\text{Y}_2\text{Mo}_2\text{O}_7$, where the magnetic Mo^{4+} ions interact predominantly via isotropic nearest neighbor antiferromagnetic exchange, possibly with additional weak disorder, is a distinct class of spin glass systems where frustration is mostly geometrical. A model proposed to describe such a spin glass behavior is the Heisenberg model on a pyrochlore lattice with random but strictly antiferromagnetic exchange disorder. In this paper, we provide compelling numerical evidence from extensive Monte Carlo simulations which show that the model exhibits a finite temperature spin glass transition and thus is a realization of a spin glass induced by random weak disorder from spin liquid. From our results, we are led to suggest that the spin glass state of $\text{Y}_2\text{Mo}_2\text{O}_7$ is driven by effective strong disorder.

PACS numbers: 75.40.Cx, 75.40.Mg, 75.50.Lk

Most magnetic materials develop long range magnetic order when the temperature is sufficiently low. There are, however, two prominent exceptions: spin liquid (SL) and spin glass (SG) systems. Both of them are commonly found among frustrated systems where the ordering tendency is reduced. The SL usually occurs in geometrically frustrated systems, whereas the SG arises in random frustrated systems due to competing random antiferromagnetic (AFM) and ferromagnetic (FM) couplings¹.

The $\text{Y}_2\text{Mo}_2\text{O}_7$ pyrochlore Heisenberg antiferromagnet²⁻⁴, possibly with some form of weak disorder, whose origin remains both mysterious and controversial⁵⁻⁷, does not fall in the category of conventional SG materials¹. The Heisenberg AFM model on the three-dimensional pyrochlore lattice of corner sharing tetrahedra is a classical spin liquid (CSL) with macroscopically degenerate ground states which satisfy the zero net magnetic moment ($\Phi_t = 0$) constraint on each tetrahedron⁸. This constraint leads to a gauge theory description of the CSL and the prediction of a power-law decaying spin-spin correlation function of “dipolar” form⁹. Thus, a clean Heisenberg AFM model on the pyrochlore lattice does not display a SG state. However, the macroscopic degeneracy in this model opens up the interesting possibility that weak random disorder in the spin-spin exchange interactions, so small that no competing AFM-FM coupling is present in the bare Hamiltonian, may be sufficient to induce a SG phase at nonzero temperature. The main question that we address in this paper is whether dense random weak disorder in the AFM exchange can induce a thermodynamic SG phase from a CSL as a case study of what may be occurring in $\text{Y}_2\text{Mo}_2\text{O}_7$ ²⁻⁴.

We study the Hamiltonian \mathcal{H} defined on a pyrochlore lattice first proposed by Bellier-Castella *et al.*¹⁰:

$$\mathcal{H} = \mathcal{H}_0 + \mathcal{H}_{\text{dis}}, \quad (1)$$

with $\mathcal{H}_0 = J_0 \sum_{\langle i,j \rangle} \mathbf{S}_i \cdot \mathbf{S}_j$ and $\mathcal{H}_{\text{dis}} = \sum_{\langle i,j \rangle} J_{ij}^{\text{dis}} \mathbf{S}_i \cdot \mathbf{S}_j$, where $\{\mathbf{S}_i\}$ are three component unit vectors and

summations are over nearest neighbors. \mathcal{H}_0 is the usual pyrochlore Heisenberg AFM model which displays on its own a CSL⁸ while \mathcal{H}_{dis} describes the random disorder which mimics the situation in $\text{Y}_2\text{Mo}_2\text{O}_7$ ⁷. Weak disorder here means $|J_{ij}^{\text{dis}}| \ll J_0$. We set the Boltzmann constant $k_B = 1$, and also set $J_0 = 1$ which serves as overall energy scale. The bond disorder is uniformly distributed in the range $J_{ij}^{\text{dis}} = [-W, W]$ with $W = J_0/10$ used in the calculations. We refer to \mathcal{H} in Eq.(1) as the BGHM model¹⁰.

The original work of Bellier-Castella *et al.* suggested, on the basis of measurements of the SG overlap parameter¹, that glassy behavior in \mathcal{H} sets in at a temperature roughly the same as W ¹⁰. In more recent studies, Saunders and Chalker¹¹ and Andreev *et al.*¹² computed the SG correlation function and SG susceptibility. Based on numerical data and analytic arguments, the authors of Ref. [12] suggested that there exists a thermodynamic SG transition at a nonzero temperature for arbitrary small but nonzero W .

SG simulations techniques have significantly improved over the past ten years or so¹³⁻²¹. Recent extensive Monte Carlo simulations employing these improvements¹⁷⁻²¹ have led to the revision of the old belief that the lower critical dimension, d_l , of the Edwards-Anderson (EA) isotropic Heisenberg SG model is above three¹. There is no rigorous analytic approach to determine the d_l of the BGHM model¹⁰⁻¹² and the previous MC simulations¹⁰⁻¹² do not come close to the computational standard of recent studies of the EA Heisenberg SG¹⁷⁻²¹. Thus, the analytic arguments and numerical data at hand can hardly provide convincing evidence for a thermodynamic SG phase in \mathcal{H} . The BGHM model, with its underlying CSL state in the disorder-free regime, as well as its broad relevance to the SG behavior observed in numerous geometrically frustrated magnetic materials, make it a model of fundamental significance in the field of frustrated magnetism. It is therefore important to carefully assess whether \mathcal{H} sustains a thermodynamic

SG phase at nonzero temperature, and to reach such a conclusion on the basis of numerics that approach the standard of SG simulations of EA models^{17–21}.

We first summarize the details of our MC simulations. A 16 site cubic unit cell for the pyrochlore lattice is used for generating cubic simulation cells with $N = 16L^3$ spins with $L = 4, 6, 8$. One Metropolis sweep, $2L$ over-relaxation sweeps and one parallel tempering swap¹³ is defined as one elementary MC step (MCS). The temperatures explored for each simulation are $T^{(n)} = T_{\min}\alpha^n$ where T_{\min} is the lowest temperature considered and $n \in [0, N_T - 1]$, where N_T is the number of thermal replicas. Thus the highest temperature is $T_{\max} = T_{\min}\alpha^{N_T-1}$ and $\alpha = \sqrt[N_T-1]{T_{\max}/T_{\min}}$. The error bars are sample-to-sample fluctuations calculated via the jackknife method. Table I lists the parameters used in our MC simulations.

L	T_{\min}	T_{\max}	N_T	$N_{\text{MCS}}^{\text{equil.}}$	$N_{\text{MCS}}^{\text{measurement}}$	N_{samples}
4	0.012	0.028	24	2×10^4	2×10^4	1750
6	0.012	0.028	30	4×10^4	2×10^4	1763
8	0.012	0.028	46	8×10^4	2×10^4	1613

TABLE I: Parameters of the Monte Carlo simulations.

To characterize a putative SG phase, we use a parameter defined as the overlap between two thermal replicas with the same realization of random couplings, $\{J_{ij}^{\text{dis}}\}$,

$$q_{\text{SG}}^{\mu,\nu}(\mathbf{k}) \equiv \frac{1}{N} \sum_{i=1}^N S_{i,\mu}^{(1)} S_{i,\nu}^{(2)} \exp(i\mathbf{k} \cdot \mathbf{r}_i), \quad (2)$$

where $S_{i,\mu}^{(1)}$ and $S_{i,\mu}^{(2)}$ are the spin components for replicas (1) and (2), respectively. It has been proposed that there is no SG transition in isotropic Heisenberg SG systems but that, instead, the freezing is in the chiral sector²². Latest simulations^{17–21} suggest that both chiral glass (CG) and SG transitions occur at finite temperature, but there is no consensus whether the CG critical temperature (T_{CG}) is higher or equal to that of the SG (T_{SG}). Since \mathcal{H} has isotropic Heisenberg spins, there is no obvious reason to exclude the possibility of a CG transition. To monitor CG correlations, we consider two chirality parameters. The first one is defined along bonds,

$$q_{\text{CG1}}(\mathbf{k}) \equiv \frac{1}{3N} \sum_{i=1}^N \sum_{\hat{\delta}=\hat{\epsilon}_{i,1};\hat{\epsilon}_{i,2};\hat{\epsilon}_{i,3}} \kappa_{1;i,\hat{\delta}}^{(1)} \kappa_{1;i,\hat{\delta}}^{(2)} \exp(i\mathbf{k} \cdot \mathbf{r}_i), \quad (3)$$

where $\kappa_{1;i,\hat{\delta}} = \mathbf{S}_{(i,\hat{\delta})} \cdot (\mathbf{S}_i \times \mathbf{S}_{(i,-\hat{\delta})})$. The $\hat{\epsilon}_{i,1}$, $\hat{\epsilon}_{i,2}$ and $\hat{\epsilon}_{i,3}$ are vectors pointing from site i , to its three nearest neighbor sites in the same tetrahedron; $(i, \hat{\delta})$, i , $(i, -\hat{\delta})$ are the indices for the three sites lying along the direction $\hat{\delta}$ (see Appendix). The second one is defined on the triangular faces of individual tetrahedra,

$$q_{\text{CG2}}(\mathbf{k}) \equiv \frac{1}{2N} \sum_{\omega=1}^{2N} \kappa_{2;\omega}^{(1)} \kappa_{2;\omega}^{(2)} \exp(i\mathbf{k} \cdot \tilde{\mathbf{r}}_{\omega}), \quad (4)$$

where $\kappa_{2;\omega} = \mathbf{S}_{\omega,a} \cdot (\mathbf{S}_{\omega,b} \times \mathbf{S}_{\omega,c})$; (ω, a) , (ω, b) , (ω, c) are the indices for the three sites of the triangular face ω and $\tilde{\mathbf{r}}_{\omega} = (\tilde{\mathbf{r}}_{\omega,a} + \tilde{\mathbf{r}}_{\omega,b} + \tilde{\mathbf{r}}_{\omega,c})/3$. The corresponding susceptibilities are obtained from the order parameters, $\chi_{\text{SG}}(\mathbf{k}) = N \sum_{\mu,\nu=x,y,z} [|\langle q_{\text{SG}}^{\mu,\nu}(\mathbf{k}) \rangle|^2]$; $\chi_{\text{CG1}}(\mathbf{k}) = 3N [|\langle q_{\text{CG1}}(\mathbf{k}) \rangle|^2] / \overline{\chi_1^4}$, $\chi_{\text{CG2}}(\mathbf{k}) = 2N [|\langle q_{\text{CG2}}(\mathbf{k}) \rangle|^2] / \overline{\chi_2^4}$, where $\langle \dots \rangle$ and $[\dots]$ denote the thermal average and disorder average, respectively. As the local chirality variables are not fixed to be unity as is the case of the spin variables^{19,20}, the CG1 susceptibility is normalized by $\overline{\chi_1^4} = (\overline{\chi_1^2})^2$, where $\overline{\chi_1^2} \equiv \frac{1}{3N} \sum_{i=1}^N \sum_{\hat{\delta}=\hat{\epsilon}_{i,1},\hat{\epsilon}_{i,2},\hat{\epsilon}_{i,3}} [\langle \kappa_{1;i,\hat{\delta}}^2 \rangle]$; and, similarly, the CG2 susceptibility is normalized by $\overline{\chi_2^4} = (\overline{\chi_2^2})^2$, where $\overline{\chi_2^2} \equiv \frac{1}{2N} \sum_{\omega=1}^{2N} [\langle \kappa_{2;\omega}^2 \rangle]$ (see Appendix).

Assuming that the susceptibilities follow an Ornstein-Zernike form¹⁴, the correlation lengths ξ_{SG} and $\xi_{\text{CG1,CG2}}$ can be determined via $\xi_g(L) = \frac{1}{2\sin(|\mathbf{k}|/2)} \left(\frac{\chi_g(\mathbf{0})}{\chi_g(\mathbf{k})} - 1 \right)^{1/2}$, where $g \equiv \text{SG, CG1 or CG2}$ and $\mathbf{k} \equiv 2\pi\hat{x}/L$ is one of the smallest wave vectors for system size L ^{17–21}. The ξ_g 's divided by L should be scale invariant at their respective critical point. The crossing of ξ_g/L is therefore a sensitive criterion to test for a glass transition. The correlation lengths and susceptibilities should finite-size scale as $\xi_g(L)/L = X[(T - T_g)L^{1/\nu_g}]$ and $\chi_g(T, L)L^{\eta_g-2} = Y[(T - T_g)L^{1/\nu_g}]$, respectively. To check that thermodynamic equilibrium was reached, we verified that ξ_g becomes independent of simulation time for the largest system size and lowest temperature considered.

We first present the SG and CG correlation lengths in Fig. 1. It is fairly clear from these results that the SG and CG correlation lengths for different system sizes tend to cross in a narrow range of temperatures compatible with a nonzero critical temperature for both SG and CG ($T_g \approx 0.016$).

We then employ a scaling scheme which assumes that the correlation lengths finite-size scale as the scaling function X given above and fit the data in the temperature range ($0.012 \leq T \leq 0.020$) by parametrizing X as polynomials $X(z) = \sum_{m=0,1,\dots,5} c_m (z - z_0)^m$. The merit function Δ , $\Delta \equiv \sum_{\text{MC data}} [X(z) / (\xi_{g,L}/L) - 1]^2$, is minimized numerically to obtain the coefficients c_m , z_0 , critical temperature T_g and exponent ν_g . Figure 2 shows $\xi_g(L)/L$ versus the scaling parameter $z \equiv (T - T_g)L^{1/\nu_g}$ (T_g and ν_g are listed in the caption of Fig. 2.) The scaling exponents determined both for the SG and CG are far from those of the 3D EA Ising model obtained from correlation length scaling ($\nu_{\text{SG}} \approx 2.44$)^{15,16}, but roughly comparable (within $\sim 20\%$) to those of the 3D EA Heisenberg model^{17–21,23}.

In the above scaling analyses, we assumed that there is a common crossing point for all system sizes. Realistically, the critical temperature obtained this way for fair system sizes ($N \leq 8192$) should represent an upper bound for the true critical temperature in the thermodynamic limit. For example, in the latest simulations of the 3D EA Heisenberg model, it was found that scaling correc-

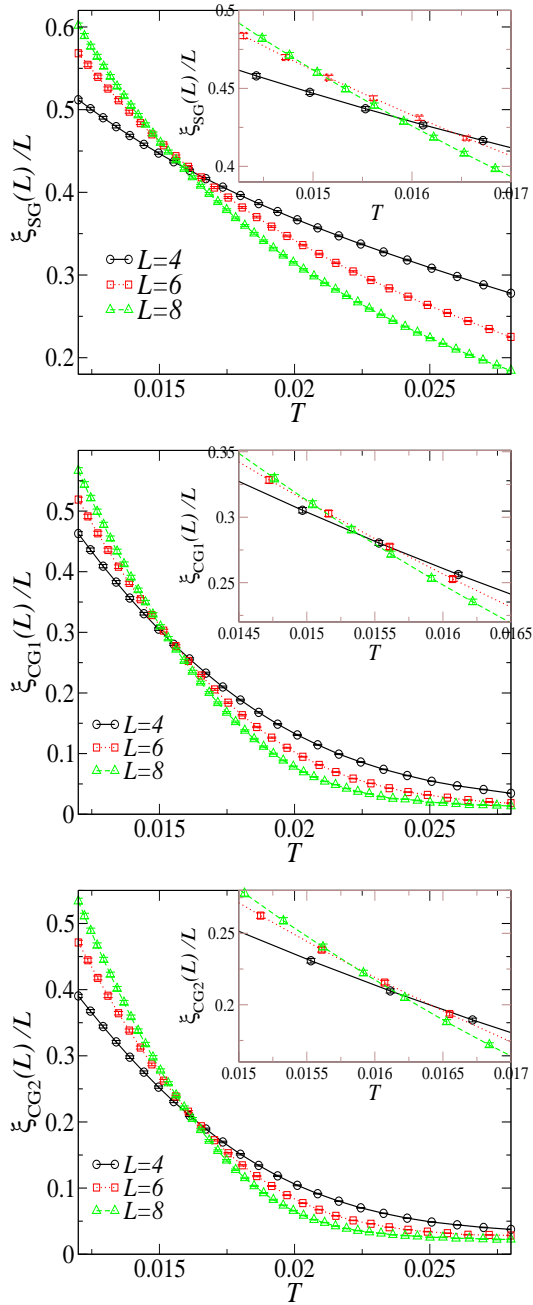


FIG. 1: (Color online). Correlation lengths for spin glass (top) and chiral glass (middle and bottom). The insets show the details close to the crossing points.

tions are large and that the ξ_g crossings are pushed to lower, albeit non-zero, temperatures as the system size increases^{17–21}. We show in Fig. 3 the evolution of the correlation lengths crossing temperatures T_g^* for different pairs of system sizes (L_1, L_2) as a function of the inverse of their average size given by $1/L_{\text{ave}} = 2/(L_1 + L_2)$. These show that $0 < T_{\text{SG}} \lesssim T_{\text{CG1}} \approx T_{\text{CG2}}$ as $L_{\text{ave}} \rightarrow \infty$.

We use the same procedure as for the correlation length data collapse to fit the susceptibilities into the scaling

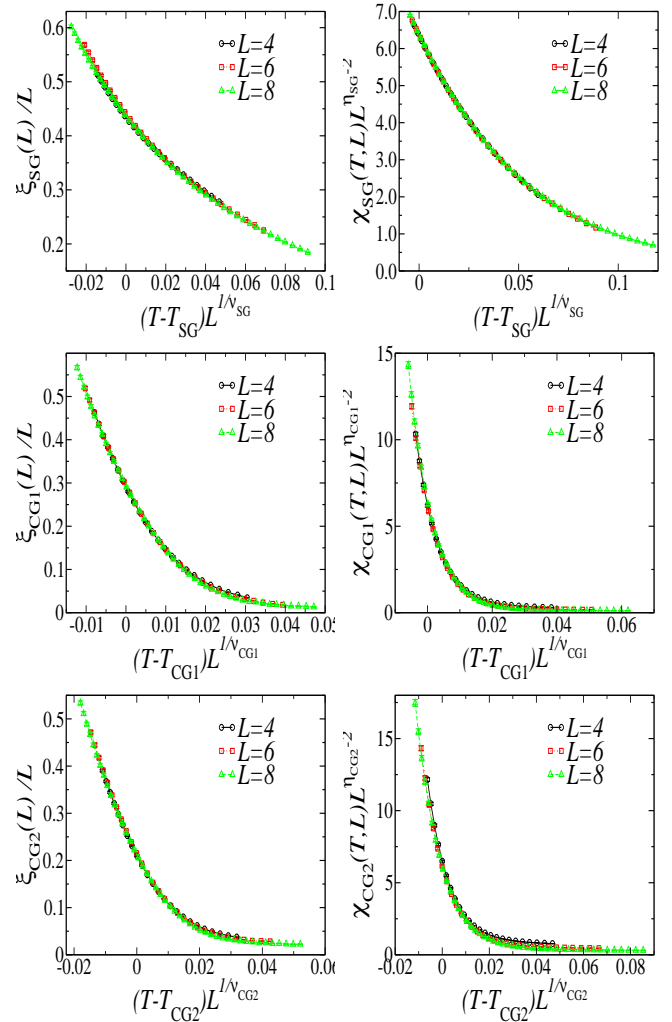


FIG. 2: (Color online). Left column: Correlation lengths for spin glass (top) and chiral glass (middle and bottom) vs $(T - T_g)L^{1/\nu_g}$. Critical temperatures and scaling exponents are $T_{\text{SG}} = 0.0157$, $\nu_{\text{SG}} = 1.037$ for SG; $T_{\text{CG1}} = 0.0153$, $\nu_{\text{CG1}} = 1.585$ and $T_{\text{CG2}} = 0.0161$, $\nu_{\text{CG2}} = 1.408$ for CG, obtained by fitting the data to the scaling function X . Right column: $\chi_g(T, L)L^{\eta_g-2}$ for spin glass (top) and chiral glass (middle and bottom) vs $(T - T_g)L^{1/\nu_g}$. Critical temperatures and scaling exponents are $T_{\text{SG}} = 0.0126$, $\nu_{\text{SG}} = 1.024$, $\eta_{\text{SG}} = -0.292$ for SG; $T_{\text{CG1}} = 0.0134$, $\nu_{\text{CG1}} = 1.439$, $\eta_{\text{CG1}} = 0.621$ and $T_{\text{CG2}} = 0.0139$, $\nu_{\text{CG2}} = 1.155$, $\eta_{\text{CG2}} = 0.698$ for CG, obtained by fitting the data to the scaling function Y . The numbers listed are the actual values used in these scaling plots. Corrections to scaling are expected to be sizable, therefore no error bar is provided, while the exponents lie within the range estimated for the 3D EA Heisenberg model.

function, Y , in order to determine T_g , ν_g and η_g . Figure 2 shows $\chi_g(T, L)L^{\eta_g-2}$ versus the scaling parameter $z = (T - T_g)L^{1/\nu_g}$. (The T_g , ν_g , and η_g are listed in the caption of Fig. 2.) The η_g and ν_g values are again fairly comparable with those obtained in the latest studies of the 3D EA Heisenberg model^{17–21,23}, providing evidence for a common SG universality class for the BGHM model

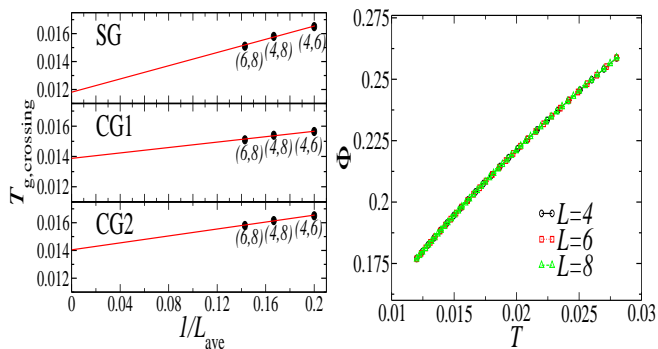


FIG. 3: (Color online). Left: Correlation length crossing temperatures for SG, CG1 and CG2 for different pairs of system sizes (L_1, L_2) . The vertical axes are the crossing temperatures and the horizontal axis is the inverse of the average system sizes given by $1/L_{\text{ave}} = 2/(L_1 + L_2)$. The lines are guides for linear extrapolations to the limit $L_{\text{ave}} \rightarrow \infty$, that is assuming $T_g^*(L_1, L_2) - T_g \propto L_{\text{ave}}^{-\theta}$ with $\theta = 1$. Right: The average tetrahedra moment, Φ , vs temperature, T .

and the 3D EA Heisenberg model.

A recent study aimed at describing the SG in \mathcal{H} assumes that the power-law correlation of the CSL⁹ is maintained despite the random disorder and thus the spins can be thought of as interacting via an effective projected interaction matrix of a long range “dipolar” form^{11,12} as a consequence of the zero net magnetic moment ($\Phi_t=0$) condition on each tetrahedron. To investigate this description, we calculate the average tetrahedra moment, $\Phi \equiv \left[\left\langle \frac{\sum_t |\sum_{i=1, \dots, 4} S(t, i)|}{N_{\text{tetrahedron}}} \right\rangle \right]$, where the outer sum is over all tetrahedra, the inner sum is over the four spins in each tetrahedron, and $N_{\text{tetrahedron}} = N/2$ is the total number of tetrahedra. We show Φ as a function of temperature in Fig. 3. First, we find that it changes very little with system size, as it is not a critical quantity. Second, it decreases with decreasing temperature. Most importantly, near the crossing temperatures ($T_g \approx 0.016$), Φ is finite and of the order of W/J_0 which implies the existence of “defect” tetrahedra with $\Phi_t \neq 0$ and, consequently, the destruction of infinite-range power-law correlations⁹. This is further supported by the reasonably good data collapse for the ξ_g correlation lengths extracted from an Ornstein-Zernike form, which would likely not be correct if there were a CSL phase with extended power-law correlations intervening between the paramagnetic phase and the SG phase.

For $\text{Y}_2\text{Mo}_2\text{O}_7$, the experimentally determined Curie-Weiss and SG temperatures are $\Theta_{\text{CW}}^{\text{exp.}} \approx -200 \text{ K}$ ^{2,3} and $T_{\text{SG}}^{\text{exp.}} \approx 22.5 \text{ K}$ ⁴, respectively. The nearest neighbor coordination number on the pyrochlore lattice is $z = 6$ and the spin S of magnetic Mo^{4+} is $S = 1$. Therefore, with $J_0 \sim J_0^{\text{mic.}} S^2$ and $\Theta_{\text{CW}}^{\text{exp.}} = J_0^{\text{mic.}} z S(S+1)/3 \approx 200 \text{ K}$, we get $J_0^{\text{mic.}} \approx 50 \text{ K}$ and the ratio $T_{\text{SG}}^{\text{exp.}} / (J_0^{\text{mic.}} S^2) \approx 0.45$. This is much higher than that obtained for the BGHM model for which we found above $T_{\text{SG}}/J_0 \sim 0.01 - 0.02$ for $W/J_0 = 0.1$. This suggests that the glass transition

of $\text{Y}_2\text{Mo}_2\text{O}_7$ is not due to weak random disorder as in \mathcal{H} , but rather to *very strong effective* disorder. One plausible scenario is that perturbations beyond nearest-neighbor Heisenberg exchange J_0 disrupt the perfect degeneracy of the CSL phase and induce short range AFM order above T_g , as observed in a neutron scattering study³. If the growth of AFM order is forestalled due to some form of random disorder⁵⁻⁷, the SG behavior of $\text{Y}_2\text{Mo}_2\text{O}_7$ should likely be described in terms of a “cluster-glass” model¹.

In conclusion, our MC simulations of the BGHM model of Eq. (1) provide compelling evidence for a thermodynamic SG phase induced by weak random disorder in a classical spin liquid of a highly frustrated system. From our work, it appears very likely that the SG behavior in $\text{Y}_2\text{Mo}_2\text{O}_7$ is not due to weak and dense random disorder but rather via an effective strong disorder whose microscopic origin requires further investigation.

This work was funded by the NSERC of Canada, the Canada Research Chair Program (M.G., Tier 1) and SHARCNET. We thank H. Kawamura for encouraging us in studying this problem and for his useful comments on our manuscript, and J. Chalker, P. Holdsworth, P. McClarty and P. Stasiak for useful discussions.

Appendix A: Spin and Chiral Glass Susceptibilities

This appendix discusses the details of the definitions of the spin glass (SG) and two different chiral glass (CG) overlap parameters – CG1 defined along the bonds and CG2 defined on the triangular faces of the tetrahedra that from a pyrochlore lattice. In addition, a table for critical exponents obtained from previous Monte Carlo studies of the three-dimensional (3D) Edwards-Anderson (EA) Heisenberg SG model is provided for comparison with the critical exponents obtained for the BGHM model studied in this paper.

The spin glass (SG) overlap is defined as the overlap between two thermal replicas with the same realization of random couplings $\{J_{ij}^{\text{dis}}\}$,

$$q_{\text{SG}}^{\mu, \nu}(\mathbf{k}) \equiv \frac{1}{N} \sum_{i=1}^N S_{i, \mu}^{(1)} S_{i, \nu}^{(2)} \exp(i\mathbf{k} \cdot \mathbf{r}_i), \quad (\text{A1})$$

where $S_{i, \mu}^{(1)}$ and $S_{i, \mu}^{(2)}$ are the spin components of the two replicas. For Ising spins, this is the usual parameter used to monitor the spin freezing. The situation is, however, more complicated for Heisenberg spins²².

It has been proposed that there is no SG transition in isotropic Heisenberg SG systems but, instead, that the freezing is in the chiral sector²². There have been many investigations on the spin-chirality coupling/decoupling scenario for the 3D EA Heisenberg model^{19-22,24-35}, but there is so far no consensus^{17-21,30}. While recent studies tend to agree that both the critical temperature for SG (T_{SG}) and chiral glass (T_{CG}) are non-zero¹⁷⁻²¹, whether $T_{\text{CG}} = T_{\text{SG}}$ ^{17,21} or $T_{\text{CG}} > T_{\text{SG}}$ ^{19,20} is still under active

debate. Since the model we study possesses spins with isotropic Heisenberg exchange, there is no a priori reason to rule out the possibility of a chiral glass (CG) transition.

To monitor the CG we probe two different chirality variables. The first one is defined along the bonds. This is a generalization of the definition of chirality variables for the 3D EA Heisenberg model on a simple cubic lattice. Similarly to the simple cubic lattice, there are three axes passing through each site. As three spins are needed to define the chirality, the natural choice is to pick a spin and its two nearest neighbors spins along one of the axes to define a chirality variables. As there are three axes passing through each site, therefore there are three chirality variables for each site. We denote this definition of chirality overlap as CG1.

$$q_{\text{CG1}}(\mathbf{k}) \equiv \frac{1}{3N} \sum_{i=1}^N \sum_{\hat{\delta}=\hat{\epsilon}_{i,1},\hat{\epsilon}_{i,2},\hat{\epsilon}_{i,3}} \kappa_{1;i,\hat{\delta}}^{(1)} \kappa_{1;i,\hat{\delta}}^{(2)} \exp(i\mathbf{k} \cdot \mathbf{r}_i) \quad (\text{A2})$$

where $\kappa_{1;i,\hat{\delta}} = \mathbf{S}_{(i,\hat{\delta})} \cdot (\mathbf{S}_i \times \mathbf{S}_{(i,-\hat{\delta})})$. The $\hat{\epsilon}_{i,1}$, $\hat{\epsilon}_{i,2}$ and $\hat{\epsilon}_{i,3}$ are vectors pointing from site i , to its three nearest neighbor sites in the same tetrahedron, see Fig. 4. $(i, \hat{\delta}), i, (i, -\hat{\delta})$ are the indices for the three sites lying along $\hat{\delta}$. The normalization factor $1/3N$ is introduced to account for the $3N$ chirality variables for this definition because of the three chirality variables at each site. We note that a slightly different definition, which treats the CG overlap as a three components object has been used in a study of 3D EA Heisenberg model²¹.

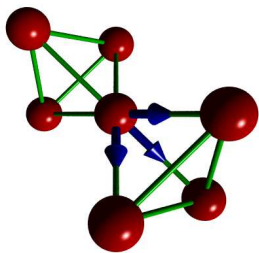


FIG. 4: (Color online). The figure illustrates the vectors for defining the chirality at one of the sites. The blue color arrows show the direction of the vectors $\hat{\epsilon}_{i,1}$, $\hat{\epsilon}_{i,2}$ and $\hat{\epsilon}_{i,3}$ for the site i (in the middle) shared by two tetrahedra.

The second chirality overlap parameter is defined on the triangular faces of the tetrahedra. The pyrochlore lattice is composed of corner-sharing tetrahedra, and each tetrahedron has 4 triangular faces. Therefore, another natural choice is to define the chirality variables on each face of the tetrahedra. In a lattice with N sites, there are $N/2$ tetrahedra, and each tetrahedron has 4 faces. Therefore, there are in total $2N$ chirality variables within this definition. We denote this definition of chirality as CG2,

with:

$$q_{\text{CG2}}(\mathbf{k}) \equiv \frac{1}{2N} \sum_{\omega=1}^{2N} \kappa_{2;\omega}^{(1)} \kappa_{2;\omega}^{(2)} \exp(i\mathbf{k} \cdot \tilde{\mathbf{r}}_{\omega}), \quad (\text{A3})$$

where $\kappa_{2;\omega} = \mathbf{S}_{\omega,a} \cdot (\mathbf{S}_{\omega,b} \times \mathbf{S}_{\omega,c})$; $(\omega, a), (\omega, b), (\omega, c)$ are the indices for the three sites of the triangular face ω and $\tilde{\mathbf{r}}_{\omega} = (\tilde{\mathbf{r}}_{\omega,a} + \tilde{\mathbf{r}}_{\omega,b} + \tilde{\mathbf{r}}_{\omega,c})/3$. The normalization factor $1/2N$ is introduced to account for the $2N$ chirality variables for this definition since there are $2N$ triangular faces.

The corresponding susceptibilities are obtained from the above order parameters,

$$\chi_{\text{SG}}(\mathbf{k}) = N \sum_{\mu,\nu=x,y,z} [|\langle q_{\text{SG}}^{\mu,\nu}(\mathbf{k}) \rangle|^2]; \quad (\text{A4})$$

$$\chi_{\text{CG1}}(\mathbf{k}) = 3N [|\langle q_{\text{CG1}}(\mathbf{k}) \rangle|^2] / \overline{\chi_1^4}, \quad (\text{A5})$$

$$\chi_{\text{CG2}}(\mathbf{k}) = 2N [|\langle q_{\text{CG2}}(\mathbf{k}) \rangle|^2] / \overline{\chi_2^4}, \quad (\text{A6})$$

where $\langle \dots \rangle$ and $[\dots]$ denote the thermal average and disorder average respectively. As the local chirality variables are not fixed to be unity in contrast of the spin variables^{19,20,35}, the CG1 susceptibility is normalized by $\overline{\chi_1^4} = (\overline{\chi_1^2})^2$, where

$$\overline{\chi_1^2} \equiv \frac{1}{3N} \sum_{i=1}^N \sum_{\hat{\delta}=\hat{\epsilon}_{i,1},\hat{\epsilon}_{i,2},\hat{\epsilon}_{i,3}} [\langle \kappa_{1;i,\hat{\delta}}^2 \rangle], \quad (\text{A7})$$

and the CG2 susceptibility is normalized by $\overline{\chi_2^4} = (\overline{\chi_2^2})^2$, where

$$\overline{\chi_2^2} \equiv \frac{1}{2N} \sum_{\omega=1}^{2N} [\langle \kappa_{2;\omega}^2 \rangle]. \quad (\text{A8})$$

The exponents obtained for the BGHM model are fairly comparable with that of the 3D EA Heisenberg spin glass model³⁶. For comparison of our results with the 3D EA Heisenberg model, we compile a selection of critical temperatures and critical exponents in Table II. For the 3D EA Ising model, see Table I in Ref. [15].

reference	randomness type	T_{SG}	ν_{SG}	η_{SG}	T_{CG}	ν_{CG}	η_{CG}
Kawamura ²⁹ (1998)	Gaussian	NA	NA	NA	0.157 ± 0.01	NA	NA
Hukushima and Kawamura ³⁴ (2000)	Gaussian	NA	NA	NA	0.160 ± 0.005	1.2	0.8
Endoh, <i>et al.</i> ³⁷ (2001)	Bimodal	0.19 ± 0.02	NA	NA	NA	NA	NA
Matsubara, <i>et al.</i> ³⁸ (2001)	Bimodal	0.18	NA	NA	NA	NA	NA
Nakamura and Endoh ³⁹ (2002)	Bimodal	$0.21^{+0.01}_{-0.03}$	1.1 ± 0.2	0.27 [#]	$0.22^{+0.01}_{-0.04}$	NA	NA
Lee and Young ¹⁷ (2003)	Gaussian	0.16 ± 0.02	1.1 ± 0.2	NA	$T_{CG} = T_{SG}$	1.3 ± 0.3	NA
Nakamura, <i>et al.</i> ⁴⁰ (2003)	Bimodal	0.20 ± 0.02	0.8 ± 0.2	-0.375 [#]	NA	NA	NA
Hukushima and Kawamura ³⁵ (2005)	Bimodal	NA	NA	NA	0.19 ± 0.01	1.3 ± 0.2	0.8 ± 0.2
Viet and Kawamura ²⁰ (2009)	Gaussian	$0.125^{+0.006}_{-0.012}$	NA	$\lesssim -0.30$	0.143 ± 0.003	1.4 ± 0.2	0.6 ± 0.2
Fernandez, <i>et al.</i> ²¹ (2009)	Gaussian	$0.120^{+0.010}_{-0.004}$	$1.49 \pm 0.13^*$	$-0.19 \pm 0.02^*$	$T_{CG} = T_{SG}$	$1.30 \pm 0.08^*$	$0.56 \pm 0.04^*$
This work (ξ/L scaling)	pyrochlore $\pm 0.1J_0$ uniform	0.0157	1.037	NA	0.0153(CG1) 0.0161(CG2)	1.585(CG1) 1.408(CG2)	NA
This work (χ scaling)	pyrochlore $\pm 0.1J_0$ uniform	0.0126	1.024	-0.292	0.0134(CG1) 0.0139(CG2)	1.439(CG1) 1.155(CG2)	0.621(CG1) 0.698(CG2)

TABLE II: Selection of critical temperatures and exponents of the three-dimensional Edwards-Anderson Heisenberg model for the simple cubic lattice. For the Edwards-Anderson Ising model see Table I in Ref. [15]. NA is a shorthand for not available. The last two rows are the estimates from this work. The variance of the random coupling distribution is 1 for all the studies on the three-dimensional Edwards-Anderson Heisenberg model listed in this table, and the variance of the model we study is $1/3 \times 10^{-2}$. (The variance is defined as $\int (x - \bar{x})^2 P(x) dx$, where $P(x)$ is the distribution function and $\bar{x} = \int x P(x) dx$.) The entries with “#” are not quoted in the original paper but are estimated via the relation $\gamma = (2 - \eta)\nu$. The entries with “*” are from the quotient method^{41,42} for scaling analysis of $L = 24$ and $L = 48$ systems on a simple cubic lattice.

-
- ¹ K. Binder and A. P. Young, Rev. Mod. Phys. **58**, 801 (1986).
² J. E. Greedan, M. Sato, X. Yan and F. S. Razavi, Solid State Commun. **59**, 895 (1986); N. P. Raju, E. Gmelin and R. K. Kremer, Phys. Rev. B **46**, 5405 (1992).
³ J. S. Gardner, S. R. Dunsiger, B. D. Gaulin, M. J. P. Gingras, J. E. Greedan, R. F. Kiefl, M. D. Lumsden, W. A. MacFarlane, N. P. Raju, J. E. Sonier, I. Swainson and Z. Tun, Phys. Rev. Lett. **83**, 211 (1999).
⁴ M. J. P. Gingras, C. V. Stager, N. P. Raju, B. D. Gaulin and J. E. Greedan, Phys. Rev. Lett. **78**, 947 (1997).
⁵ C. H. Booth, J. S. Gardner, G. H. Kwei, R. H. Heffner, F. Bridges and M. A. Subramanian, Phys. Rev. B **62**, R755 (2000).
⁶ A. Keren and J. S. Gardner, Phys. Rev. Lett. **87**, 177201 (2001); E. Sagi, O. Ofer, A. Keren and Jason S. Gardner, Phys. Rev. Lett. **94**, 237202 (2005).
⁷ J. E. Greedan, D. Gout, A. D. Lozano-Gorrin, S. Derahkshan, Th. Proffen, H.-J. Kim, E. Božin and S. J. L. Billinge, Phys. Rev. B **79**, 014427 (2009).
⁸ J. N. Reimers, A. J. Berlinsky and A.-C. Shi, Phys. Rev. B **43**, 865 (1991); J. N. Reimers, Phys. Rev. B **45**, 7287 (1992); R. Moessner and J. T. Chalker, Phys. Rev. Lett. **80**, 2929 (1998).
⁹ S. V. Isakov, K. Gregor, R. Moessner and S. L. Sondhi, Phys. Rev. Lett. **93**, 167204 (2004); C. L. Henley, Phys. Rev. B **71**, 014424 (2005).
¹⁰ L. Bellier-Castella, M. J. P. Gingras, P. C. W. Holdsworth and R. Moessner, Can. J. Phys. **79**, 1365 (2001).
¹¹ T. E. Saunders and J. T. Chalker, Phys. Rev. Lett. **98**, 157201 (2007).
¹² A. Andreanov, J. T. Chalker, T. E. Saunders and D. Sherrington, Phys. Rev. B **81**, 014406 (2010).
¹³ K. Hukushima and K. Nemoto, J. Phys. Soc. Jpn. **65**, 1604 (1996); E. Marinari and G. Parisi, Europhys. Lett. **19**, 451 (1992).
¹⁴ H. G. Ballesteros, A. Cruz, L. A. Fernández, V. Martín-Mayor, J. Pech, J. J. Ruiz-Lorenzo, A. Tarancón, P. Téllez, C. L. Ullod and C. Ungil Phys. Rev. B **62**, 14237 (2000).
¹⁵ H. G. Katzgraber, M. Körner and A. P. Young, Phys. Rev. B **73**, 224432 (2006).
¹⁶ M. Hasenbusch, A. Pelissetto and E. Vicari, Phys. Rev. B **78**, 214205 (2008).
¹⁷ L. W. Lee and A. P. Young, Phys. Rev. Lett. **90**, 227203 (2003).
¹⁸ L. W. Lee and A. P. Young, Phys. Rev. B **76**, 024405

- (2007).
- ¹⁹ D. X. Viet and H. Kawamura, Phys. Rev. Lett. **102**, 027202 (2009).
- ²⁰ D. X. Viet and H. Kawamura, Phys. Rev. B **80**, 064418 (2009).
- ²¹ L.A. Fernández, V. Martín-Mayor, S. Perez-Gaviro, A. Tarancón, A.P. Young, Phys. Rev. B **80**, 024422 (2009).
- ²² H. Kawamura, Phys. Rev. Lett. **68**, 3785 (1992).
- ²³ See Appendix.
- ²⁴ H. Kawamura and M. Tanemura, J. Phys. Soc. Jpn. **60**, 608 (1991).
- ²⁵ H. Kawamura, Phys. Rev. B **51**, 12398 (1995).
- ²⁶ H. Kawamura and M. Tanemura, Phys. Rev. B **36**, 7177 (1987).
- ²⁷ H. Kawamura, J. Phys. Soc. Jpn. **64**, 26 (1995).
- ²⁸ H. Kawamura and K. Hukushima, J. Magn. Magn. Mater. **177**, 69 (1998).
- ²⁹ H. Kawamura, Phys. Rev. Lett. **80**, 5421 (1998).
- ³⁰ H. Kawamura, J. Phys. Soc. Jpn. **79**, 011007 (2010).
- ³¹ H. Kawamura, J. Phys.: Conf. Ser. **233**, 012012 (2010).
- ³² I. A. Campbell and D. C. M. C. Petit, J. Phys. Soc. Jpn. **79**, 011006 (2010).
- ³³ D. Petit, L. Fruchter and I. A. Campbell, Phys. Rev. Lett. **88**, 207206 (2002).
- ³⁴ K. Hukushima and H. Kawamura, Phys. Rev. E **61**, R1008 (2000).
- ³⁵ K. Hukushima and H. Kawamura, Phys. Rev. B **72**, 144416 (2005).
- ³⁶ S. F. Edwards and P. W. Anderson, J. Phys. F: Metal Phys. **5**, 965 (1975).
- ³⁷ S.-i. Endoh, F. Matsubara and T. Shirakura, J. Phys. Soc. Jpn. **70**, 1543 (2001).
- ³⁸ F. Matsubara, T. Shirakura and S. Endoh, Phys. Rev. B **64**, 092412 (2001).
- ³⁹ T. Nakamura and S.-i. Endoh, J. Phys. Soc. Jpn. **71**, 2113 (2002).
- ⁴⁰ T. Nakamura S.-i. Endoh and T. Yamamoto, J. Phys. A: Math. Gen. **36**, 10895 (2003).
- ⁴¹ K. Binder, Z. Phys. B: Condens. Matter **43**, 119 (1981).
- ⁴² H. G. Ballesteros, L. A. Fernández, V. Martín-Mayor and A. Muñoz Sudupe, Phys. Lett. B **387**, 125 (1996).